Strike-slip motion and double ridge formation on Europa

Francis Nimmo

Department of Geological Sciences, University College London, London, UK

Eric Gaidos

Department of Geology and Geophysics, University of Hawaii, Honolulu, Hawaii, USA

Received 26 February 2001; revised 12 November 2001; accepted 3 December 2001; published 16 April 2002.

[1] There is abundant observational evidence for strike-slip displacement on the surface of Europa. Strike-slip motion between crustal blocks produces shear heating and an increase in temperature. We model the shear heating within the ice crust using a two-dimensional, finite difference formulation, with a near-surface brittle layer of constant specified thickness and a Newtonian ductile layer beneath. We obtain a maximum temperature anomaly of 66 K for a brittle layer thickness of 2 km and shear velocity of 6×10^{-7} m s^{-1}. Such a velocity is appropriate for diurnal (85 hour) tidal motion. The local increase in temperature may cause $\sim$100 m uplift around the shear zone through thermal buoyancy. The stresses required to produce velocities of order 10^{-7} m s^{-1} are similar to estimates for present-day tidal stresses on Europa (10^4–10^5 Pa). Brittle layer thicknesses >2 km are unlikely to persist at active shear zones because of the effect of shear heating. Shear velocities greater than or equal to $\sim 10^{-6}$ m s^{-1} will give rise to melting at shallow depths. The removal of material by downwards percolation of meltwater may cause surface collapse along the shear zone; inward motion, leading to compression, may also result. The combination of thermally or compression-induced uplift and melt-related collapse may be responsible for the pervasive double ridges seen on Europa's surface. *INDEX TERMS:* 5475 Planetology: Solid Surface Planets: Tectonics (8149); 6218 Planetology: Solar System Objects: Jovian satellites; 8120 Tectonophysics: Dynamics of lithosphere and mantle—general; 8160 Tectonophysics: Rheology—general; *KEYWORDS:* ice, shear zone, melting, viscosity, brittle-ductile transition

1. Introduction

[2] On the Earth the movement of plates creates areas in which relative lateral motion occurs. Such shear zones occur at strike-slip plate boundaries and also at subduction zones [*Yuen et al.*, 1978]. Near the surface this motion is confined to a fault plane, but at depth it is likely to be accomplished by ductile flow. In both cases, shear heating may result. In the ductile regime it has long been recognized [*Turcotte and Oxburgh*, 1968] that this heating may reduce the viscosity of the deforming material and thus alter the heat generation rate, leading to feedback. Under certain circumstances the feedback is positive, and a thermal runaway may occur, possibly resulting in melt generation.

[3] Convincing evidence has been presented for the existence of strike-slip zones with displacements of 1–10 km on Europa [*Tufts et al.*, 1999; *Hoppa et al.*, 2000]. Such motion is a plausible result of the accommodation of tidal strain in a crust broken into mobile, rigid blocks and will have an amplitude of $\sim$1 m for present-day diurnal tides [*Greenberg et al.*, 1998]. Double ridges are usually associated with areas of strike-slip motion [*Hoppa et al.*, 2000]. These ridges consist of paired rises, 1–2 km apart with an elevation of $\sim$100 m and a central valley between [*Head et al.*, 1999; *Giese et al.*, 1999].

[4] In this paper we extend the work of *Stevenson* [1996] and *Gaidos and Nimmo* [2000] to explore the quantitative consequences of strike-slip motion and investigate the circumstances under which the generation of melt may occur. We also suggest a mechanism by which strike-slip motion may lead to the formation of double ridges.

2. Theory

[5] The stress τ_d required to produce ductile flow in silicate or icy materials can be described by the stress-strain rate relationship [*Durham et al.*, 1997]

$$\tau_d = \left(\frac{\dot{\epsilon}}{A}\right)^{1/n} \exp(Q/nRT), \tag{1}$$

where $\dot{\epsilon}$ is the strain rate, n is a constant, Q is the activation energy, R is the gas constant, T is the temperature, A may be constant or a function of T, and the effects of grain size dependence are neglected.

[6] This stress is clearly strongly temperature-dependent. Conversely, the shear stress τ_f required to cause motion on a preexisting planar surface (a fault) is given by

$$\tau_f = \mu\sigma, \tag{2}$$

where σ is the normal stress on the fault and μ is the coefficient of friction. The material will move by whichever mechanism requires lower stress: at shallow levels, where temperatures are cold, deformation will be accomplished by brittle motion; at greater depths, viscous flow will occur. On Earth the depth at which the transition from brittle to ductile deformation occurs [*Brace and Kohlstedt*, 1980] has been linked to the observed depth distribution of crustal earthquakes [*Sibson*, 1982; *Chen and Molnar*, 1983].

0148-0227/02/2000JE001476$09.00

The temperature at which the transition occurs will be referred to as T_D. The depth to the brittle-ductile transition increases with increasing strain rate but decreases with increasing thermal gradient. *Pappalardo et al.* [1999] estimated that T_D for Europa was 180–200 K for a strain rate of 2×10^{-10} s^{-1}, depending on thermal gradient, and *Golombek and Banerdt* [1990] obtained values of around 120 K at a strain rate of 10^{-15} s^{-1}.

[7] In the brittle part of the crust the heat generated per unit area H_f by shear motion on a fault plane is given by

$$H_f = \mu\rho g z u, \tag{3}$$

where ρ is the density, g is the acceleration due to gravity, z is the depth below the surface, and u is the shear velocity. Note that we are assuming that the dynamical friction coefficient μ is the same as for equation (2). For a fault plane that extends to a depth D within a semi-infinite medium, the maximum temperature rise ΔT in steady state occurs at the base of the fault and is given by *Stevenson* [1996]

$$\Delta T = \frac{\mu\rho g D^2 u_0}{2\pi k}, \tag{4}$$

where k is the thermal conductivity and u_0 is the velocity change across the fault.

[8] In the ductile part of the crust the heating H_v per volume of a viscous fluid undergoing shear is given by

$$H_v = \eta\left(\frac{\partial u}{\partial x}\right)^2, \tag{5}$$

where η is the effective viscosity. For a time-dependent velocity the above equation describes the time-averaged heat generation rate if the RMS velocity is used. This heat generation rate will produce an increase in temperature within the shear zone. The viscosity of most geological materials, including ice, tends to decrease with increasing temperature. Thus the temperature will reach some equilibrium value at which H_v is balanced by conduction of heat out of the zone. If the stress, rather than the velocity, is specified, the shear heating may lead to a thermal runaway [*Lockett and Kusznir*, 1982].

[9] Within the ductile zone, and neglecting an inertial term, the steady state horizontal velocity field is defined by

$$\nabla(\eta\nabla u) = 0. \tag{6}$$

[10] The effective viscosity of ice, ($=\tau_d/\dot{\epsilon}$), can be defined using equation (1). However, to allow comparison with the analytical solution of *Yuen et al.* [1978] (see below), we adopt the following form for the viscosity

$$\eta = \frac{T}{2B}\exp(Q/RT), \tag{7}$$

where B is a constant and other terms are defined above. This simplified form is equivalent to assuming that $n = 1$ in equation (1), i.e., that the material is Newtonian.

[11] Given the shear heating, the evolution of the temperature field, T, may be calculated. The shearing velocity is perpendicular to the plane of interest, and in two dimensions we assume that the vertical component of velocity is small (see section 6). We therefore ignore advection and write

$$\frac{\partial T}{\partial t} = \kappa\nabla^2 T + \frac{H}{\rho C_p}, \tag{8}$$

where C_p is the specific heat capacity, κ is the thermal diffusivity, and H is the heat generation per unit volume.

[12] In a purely viscous case, given a set of boundary conditions, equations (6), (7), and (8) can be solved to calculate the evolution of velocity and temperature with time [*Yuen et al.*, 1978; *Fleitout and Froidevaux*, 1980; *Lockett and Kusznir*, 1982; *Jacobson and Raymond*, 1998]. In rheologically complex materials such as ice the viscosity also depends on the strain rate, $\partial u/\partial x$; although analytical solutions to this more complex problem do exist [*Fleitout and Froidevaux*, 1980], for computational simplicity we have neglected this effect. It will later be shown that the viscous heating is generally minor compared to the brittle heating, and thus the rheological details are probably of secondary importance.

[13] *Yuen et al.* [1978] solved the above equations for a one-dimensional (1-D) viscous shear zone defined by $u = \pm u_0/2$ at $x = \pm\infty$ and $T = T_0$ at $t = 0$. They found that in steady state

$$u_0^2 = 16kB\left[E_1\left(\frac{Q}{RT_c}\right) - E_1\left(\frac{Q}{RT_0}\right)\right], \tag{9}$$

where T_c is the temperature at the center of the shear zone, k is the conductivity, and E_1 is the exponential integral [*Abramowitz and Stegun*, 1970]. For this geometry the lateral extent of the temperature anomaly increases with the square root of time (as expected for thermal diffusion), but the peak temperature remains constant. For cases in which $T_c \gg T_0$, and using equation (7), we obtain

$$T_c^2 = \frac{u_0^2\eta_c Q}{8kR}, \tag{10}$$

where η_c is the viscosity at the center of the shear zone. Thus the temperature rise increases with velocity and viscosity and decreases with thermal conductivity, as expected. *Fleitout and Froidevaux* [1980] show that the same formula is also a very good approximation for non-Newtonian materials.

3. Model

[14] The mean surface temperature on Europa is ~120 K [*Ojakangas and Stevenson*, 1989], whereas the base of the ice shell is around 270 K (the solidus temperature), so thermal gradients, and hence gradients of effective viscosity, must exist within the crust. Moreover, images of the surface show pervasive brittle deformation [*Pappalardo et al.*, 1999], whereas it is likely that deformation near the base of the crust will be taken up by ductile motion [*Pappalardo et al.*, 1998]. The near-surface temperature structure will be controlled by the surface boundary conditions, whereas temperatures at depth will also be influenced by lateral heat transport. We have therefore constructed a 2-D numerical model that incorporates both brittle and ductile shear heating and both vertical and lateral heat transport.

[15] Figure 1 illustrates the geometry of our model. The box width (x direction) is w, and the velocities at the two sides are $+u_0/2$ and $-u_0/2$, respectively. The thickness of the box (z direction) is h and consists of an upper, brittle layer of thickness D overlying a ductile layer. The thickness of the brittle layer is constant in both space and time. In the upper layer the velocity varies with position as a step function centered on the fault zone. To avoid this singularity, the velocity variation at the top of the ductile layer is specified to take place within a narrow zone (see below). The vertical gradient of velocity at the base of the crust is set to zero.

[16] We wish to find the steady state temperature and velocity distribution and use a finite difference method in two dimensions, where the grid spacings in the x and z directions are in general unequal. The model consists of a ductile layer, with equal numbers of nodes in the x and z directions, and a brittle layer on top with the same node spacing in x and z (see Figure 1).

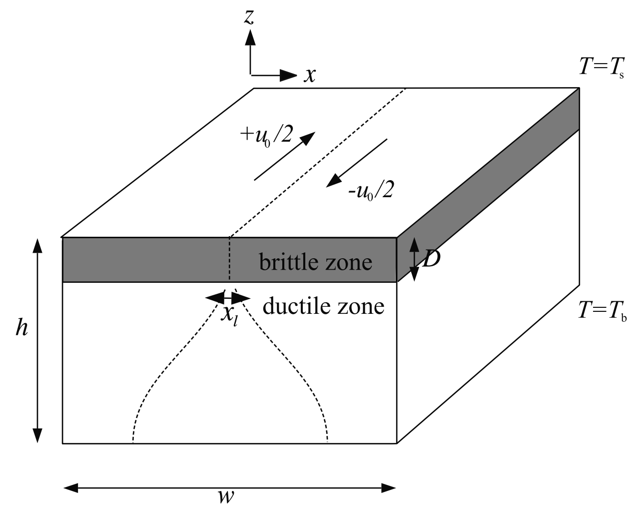

Figure 1. Diagram of model geometry. Dotted lines show approximate location of shear zone. Shaded area is brittle zone, x_l is the characteristic width of the shear zone (see equation (13)), and T_s and T_b are surface and base temperatures.

[17] We first solve for the velocity in the ductile layer (equation (6)), given the specified boundary conditions and using successive overrelaxation [*Press et al.*, 1992]. We then calculate the temperature distribution throughout the entire crust. For the ductile layer we calculate the resulting heat generation rate H using [*Jacobson and Raymond*, 1998]

$$H = \eta\left[\left(\frac{\partial u}{\partial x}\right)^2 + \left(\frac{\partial u}{\partial z}\right)^2\right]. \quad (11)$$

[18] In the brittle layer the heat generation is set to zero everywhere except the central node in each layer. For this position we calculate the heat generation rate per unit volume using (compare with equation (3))

$$H = \frac{\mu\rho g j \Delta z u_o}{\Delta x}, \quad (12)$$

where Δx and Δz are the grid spacings and j is the number of grid nodes beneath the surface. We discuss the effect of this approximation in Appendix A.

[19] The temperature field is then updated using a finite difference approximation of equation (8), with the appropriate value of H used for each node. We use an adaptive time step such that the maximum temperature change for any iteration never exceeds 0.01 K, and the time step does not exceed the Courant criterion. The updated temperature field is then used to recalculate the viscosity within the ductile layer using equation (7), and the whole process is iterated until convergence is obtained. Because the coupling between velocity and temperature is quite weak [*Jacobson and Raymond*, 1998], we updated the velocity every 100 time steps. Updating the velocity every time step resulted in a change in the final maximum temperature anomaly of <1 K.

[20] In some cases, T may exceed the melting temperature T_m, here assumed to be 270 K independent of depth. In such locations, T is fixed at T_m, and we calculate the melt generation rate by assuming that the heat generation in areas where melting occurs is balanced by the consumption of latent heat due to melting.

[21] The velocity boundary condition at the top of the ductile layer, which we also use as our initial velocity profile throughout the layer, is given by

$$u(x) = u_0 \tan^{-1}(x/x_l)/\pi, \quad (13)$$

where x_l determines the width of the surface fault zone. The vertical velocity gradient at the base of the layer is specified to be zero, and the side velocities do not change from their initial values. The initial temperature profile is conductive:

$$T(z) = T_s + z(T_b - T_s)/h, \quad (14)$$

where T_s and T_b are the temperature at the surface and base, respectively. Temperatures at the surface and base are constant and do not change from the initial conductive solution (equation (14)) at the sides.

[22] Our boundary conditions are simplified in that we assume a velocity constant in time and orientation, while the real case may include a unidirectional component superimposed on a cyclical motion at the tidal timescale [*Hoppa et al.*, 1999]. The simplified boundary conditions are probably justified as long as the velocity varies on a timescale that is fast compared to the thermal diffusion timescale.

4. Parameters

[23] Equations (4) and (10) show that the temperature rise is heavily dependent on the shear velocity. There are two deformation timescales of interest on Europa. The cyclical displacement associated with diurnal ($\sim$ 85 hours) tidal stresses may approach 1 m [*Greenberg et al.*, 1998], leading to velocities of order 10^{-6} m s^{-1}. However, the net displacement over each tidal cycle, which leads to the gradual development of strike-slip offsets [*Hoppa et al.*, 1999], may be considerably smaller. If the observed displacements of 1–10 km occur over the timescale for asynchronous rotation [*Hoppa et al.*, 1999], the velocities are of order 10^{-8} – 10^{-10} m s^{-1}, based on a rotation timescale of 10^4 – 10^5 a [*Hoppa et al.*, 2000]. We therefore investigate a range of velocities appropriate to both diurnal and asynchronous timescales.

[24] In the ductile zone, viscosity has a large effect on the temperature rise. The viscosity of ice is affected by factors such as grain size [*Durham et al.*, 1997] that are not well known for Europa. We therefore elected to define the viscosity in a simple way and then vary the important parameters over the likely range to investigate the sensitivity of our results. We define the reference viscosity η_0 as that given by equation (7) at a reference temperature, T_0. For T_0 = 250 K, η_0 for ice probably ranges from 10^{13} to 10^{15} Pa s [*Pappalardo et al.*, 1998, Figure 2]. Ice is generally non-Newtonian with a value of Q/n (see equation (1)) of 15–30 kJ mol^{-1} [*Goldsby and Kohlstedt*, 2001]. Since equation (7) assumes a Newtonian rheology (n = 1), we used Q = 20 kJ mol^{-1} and discuss the effect of varying this parameter in section 6.

[25] For brittle deformation, equation (4), D and μ are the most important variables. The coefficient of friction of ice-ice motion varies from about 0.1 to 0.6, depending on velocity and pressure [*Kennedy et al.*, 2000]. Here we adopt a value of 0.1 because it is characteristic of situations in which melting occurs and because it will provide a conservative (lower) bound on the temperature increase produced. The thickness of the brittle layer, D, has been estimated from the scales of various surface landforms to be 0.4–3 km [*Pappalardo et al.*, 1999; *McKinnon*, 2000]. Since D is probably thermally controlled, it is important to verify that the temperature structure obtained assuming a particular value of D is consistent with the likely temperature T_D that defines the brittle-ductile transition (see section 5).

Table 1. Constants Used in Numerical Calculation

Quantity	Units	Value
T_s	K	120
T_b	K	270
T_0	K	250
C_p	J kg^{-1}K^{-1}	2100
η_0	Pa s	10^{14}
μ	–	0.1
Q	kJ mol^{-1}	20
ρ	kg m^{-3}	1000
u_0	m s^{-1}	6×10^{-7}
g	m s^{-2}	1.3
x_1	km	0.3
h	km	20
w	km	30
D	km	2
k	W m^{-1}K^{-1}	2

[26] The total thickness of the ice shell is not certain. Although magnetometer data [*Kivelson et al.*, 2000] indicate that part of the shell is liquid, it does not constrain the liquid thickness. Geological observations do not distinguish between thin (~5 km) and thick (~30 km) crusts [*Pappalardo et al.*, 1999; *Carr et al.*, 1998], mainly because of the expected weakness of ice near the melting temperature.

[27] The initial values of the constants used are tabulated in Table 1, and the effect of varying them is addressed in section 6. Table 2 shows the grid spacings used for different values of D and h.

5. Results

[28] We first verified that our model could reproduce the analytical results for both purely brittle and purely ductile deformation. Further details of this step, and investigations of the sensitivity of the model to varying the grid resolution, are given in Appendix A.

[29] Figure 2 shows the results using the parameters listed in Table 1, in which D = 2 km, $\eta_0 = 10^{14}$ Pa s, and $u_o = 6 \times 10^{-7}$ m s^{-1}. This velocity is appropriate if the deformation occurs over diurnal timescales (see section 4). Figure 2a shows the velocity within the ductile layer as a function of position. The velocity field within the ductile layer is fixed by the velocity profile at the top of the ductile layer, but it becomes more broadly distributed with depth as the lateral viscosity gradient decreases. The shear heating (Figure 2b) increases with depth through the brittle zone owing to the increasing overburden pressure (equation (3)) but decreases through the viscous zone because of the reduction in viscosity and velocity gradient (equation (5)). This distribution of heat generation causes the temperature anomaly (Figure 2d) to be highest near the base of the brittle zone. The overall temperature (Figure 2c) increases toward the shear zone, as expected, and the viscosity distribution mirrors this pattern.

[30] Figure 3 shows vertical profiles of temperature and shear stress through the crust for the case shown in Figure 2. The shear stress τ at any point in the ductile layer is given by

$$\tau = \eta\left(\frac{\partial u}{\partial x}\right). \tag{15}$$

[31] The ductile shear stress can thus be calculated. In the brittle layer the shear stress is simply the product of the overburden pressure and the coefficient of dynamic friction.

[32] Figure 3a shows that the temperature anomaly is greatest around the base of the brittle layer, as is the stress. The temperature at the base of the brittle layer is around 200 K, which is similar to the brittle-ductile transition temperature of *Pappalardo et al.* [1999]. The stress decreases below the base of the brittle layer owing to the reduction in viscosity with increasing temperature. The stresses calculated (~10^5 Pa) are comparable to those estimated to arise owing to tidal forces, ~10^4–10^5 Pa [*Greenberg et al.*, 1998]. A thicker brittle layer D would increase both the maximum temperature anomaly and stress, but these maxima would still occur around the base of the brittle layer. As noted above, an increase in D would cause the model temperature at the base of the brittle layer to exceed the likely temperature T_D that defines the brittle-ductile transition. This is a point we discuss further below.

[33] Figure 2d shows that the maximum temperature anomaly is 66 K. The local surface heat flux is also elevated relative to the surroundings: the background heat flux is ~15 mW m^{-2} but increases to ~100 mW m^{-2} over the center of the shear zone. This increase is large compared to the estimated radiogenic heat flux from the silicate interior of 8 mW m^{-2} [*Schubert et al.*, 1986].

[34] Figure 2 shows that the shear heating causes the steady state isotherms at the shear zone to become more shallow. Since the thickness of the brittle layer D is in reality likely to be temperature-dependent, the temperature at depth D from the numerical modeling must eventually equal the temperature at which the brittle-ductile transition is predicted to take place from rheological arguments. The timescale over which this equalization will take place is the thermal diffusion timescale, ~$10^5 a$ for a 2 km thick brittle layer.

[35] The temperature at the base of the brittle layer T_D may be obtained by using equations (2) and (7) to find the point at which $\tau_d = \tau_f$. We calculated the viscosity as a function of depth for each model using equation (7) and the near-surface model thermal gradient and thus derived the ductile stress using $\tau_d = \eta\dot{\varepsilon}$. The strain rate ϵ is given by u_o/w (see Table 1). For the parameters in Table 1, the strain rate was 2×10^{-11} s^{-1}, and the thermal gradient was ~40 K km^{-1} and T_D = 170 K.

[36] Figure 4 shows the brittle-ductile transition temperature T_D calculated as described above for different values of η_0. As expected, T_D increases with increasing strain rate or increasing reference viscosity. Figure 4 also plots the steady state temperature at the base of the brittle zone as a function of u_0 and D for the numerical model. The temperature at the base of the brittle zone increases with D and u_0. The effect of increasing η_0 is to cause a larger increase in temperature if D is small, because viscous heating is then more important. Only those models for which the numerical calculation of the temperature at the base of the brittle layer equals T_D are stable over time. Brittle layers that are initially of greater thickness will become shallower with time owing to the heating caused by shear motion. For brittle layers thicker than 2 km the predicted temperature at D always exceeds the likely value of T_D. For brittle layers with $D \leq 2$ km there is a range of model brittle thicknesses that are compatible with the rheological constraints. As shear velocities increase, smaller brittle thicknesses are stable. Thus an important conclusion from this study is that the long-term brittle layer thickness at shear zones is unlikely to be >2 km for the range of shear velocities considered.

[37] Figure 5a plots the maximum temperature anomaly as a function of shear velocity and brittle layer thickness. At low velocities and low values of D the ductile layer is cold and viscous and thus contributes substantially to the shear heating. Under these conditions the total temperature anomaly is greater than that

Table 2. Grid Spacings Used for Different D and h

h, km	D, km	Brittle Nodes	Ductile Nodes	Δx, km	Δz, km
20	0	0	54	0.566	0.377
20	1	5	77	0.395	0.250
20	2	7	54	0.566	0.333
20	4	11	40	0.769	0.400
20	6	19	42	0.732	0.333
30	2	5	56	0.545	0.500
10	2	7	24	1.304	0.333

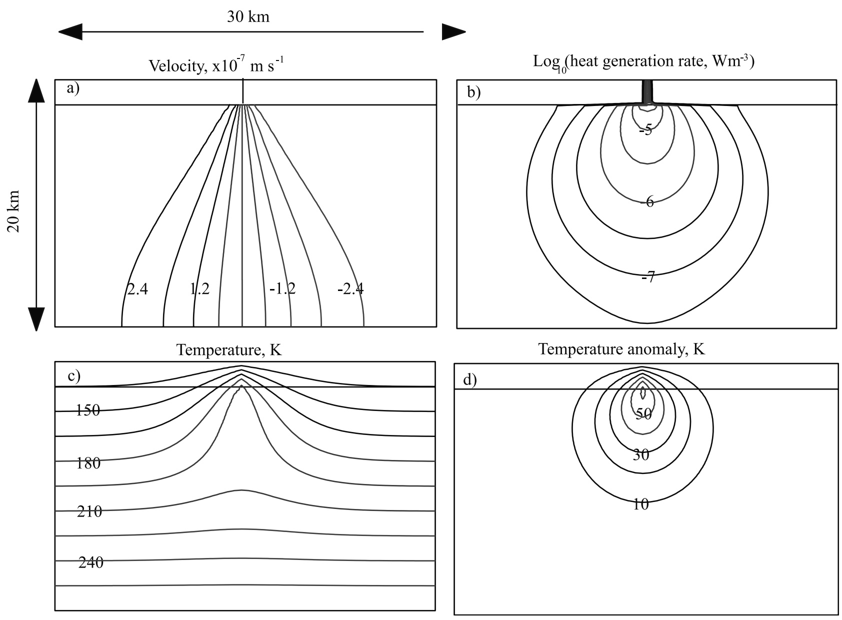

Figure 2. Cross sections perpendicular to shear plane for parameters listed in Table 1. Shear zone is at center. Box is 30 km wide and 20 km deep; brittle layer is 2 km thick. (a) Contours of velocity. Contours are evenly spaced at intervals of 0.6×10^{-7} m s^{-1}. (b) Contours of log of heat generation, evenly spaced at 0.5 log units. (c) Temperature contours. Surface temperature is 120 K, base temperature is 270 K, and contour interval is 15 K. (d) Temperature anomaly relative to conductive solution. Contour interval is 10 K; max value is 66 K.

expected from the purely brittle analytical solution (equation (4)). At higher velocities and values of D the contribution of the ductile layer becomes progressively less important; however, as was noted above, values of $D > 2$ km are unlikely to persist for long periods because the temperature at the base of the model brittle zone exceeds T_D. Figure 5a also plots the temperature anomaly for a purely viscous case ($D = 0$ in Table 2). At low shear velocities the temperature anomaly is larger than for the brittle cases because the brittle heating depends on the shear velocity (equation (3)), whereas the viscous heating depends on the velocity gradient and the viscosity (equation (5)). Both of these are high at shallow depths, where the majority of heating occurs. Figure 5b plots the effect of varying the ductile layer reference viscosity on the temperature anomaly. As expected, the lower the reference viscosity, the smaller the deviation from the purely brittle analytical solution (equation (4)).

[38] For temperature anomalies greater than ~100 K, melting is likely to occur and will be centered near the base of the brittle zone (see Figure 3a). Figure 5a shows that for $D = 0$ and $D = 1$ km, melting is likely to occur for values of $u_0 \geq \sim 10^{-6}$ m s^{-1}. Larger values of D would produce melting at slower velocities, but Figure 4 shows that these values are unlikely to be compatible with the long-term, rheologically determined depth to the brittle-ductile transition. By equating the heat generation rate in the nodes where melting occurs with the latent heat of ice, melt generation rates of $\sim 10^{-6}$–10^{-5} m^2 s^{-1} are obtained. Using a purely viscous model, *Gaidos and Nimmo* [2000] predicted similar melt generation rates for velocities of the same order. All these values are likely to be only approximate, as melting will probably alter variables such as the coefficient of friction and viscosity.

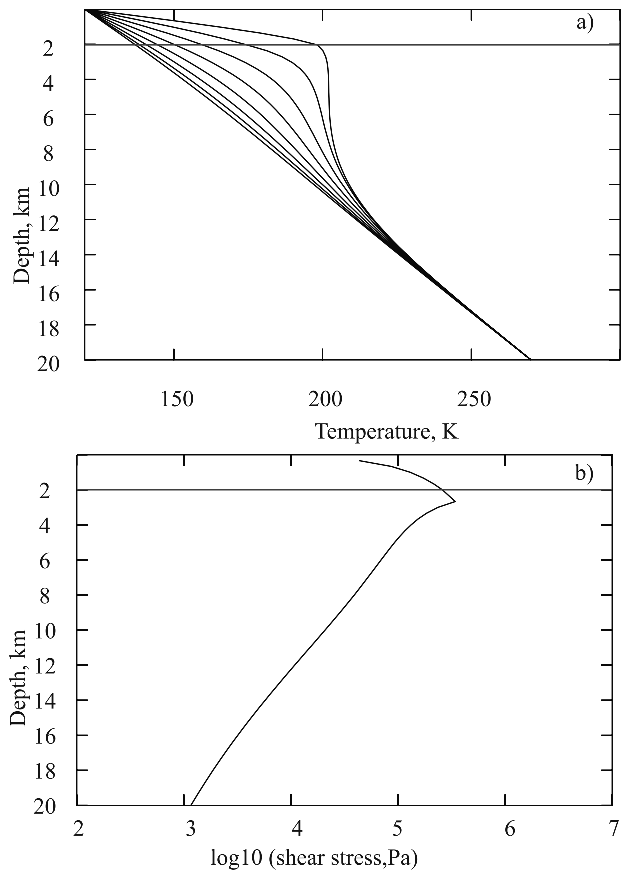

Figure 3. Temperature and stress profiles plotted at intervals from center of shear zone for $D = 2$ km and $u_0 = 6 \times 10^{-7}$ m s^{-1}. (a) Temperature profile at evenly spaced intervals from center of zone. (b) Stress profile at center of zone.

6. Discussion

[39] Figure 5a shows that shear heating is dominated by the brittle layer except at low velocities or small values of D. However, large values of D produce a temperature structure that is not likely to be stable over time, since the temperature at the base of the

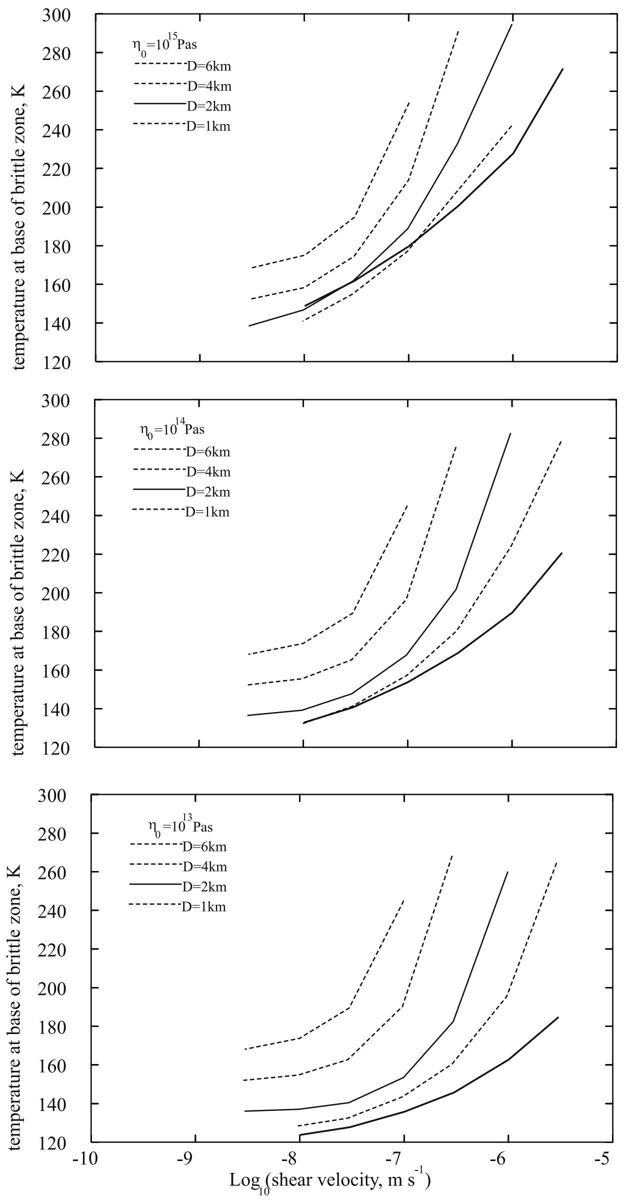

Figure 4. (a) Plot of temperature at base of brittle layer from model and rheologically determined temperature to base of brittle layer (from equations (2) and (7)). Thin lines are model results for different thicknesses of brittle layer D. Bold line is rheologically determined temperature T_D (see text). Reference viscosity η_0 is 10^{15} Pa s. Velocity plotted is $u_0/2$. (b) As for Figure 4a but for $\eta_0 = 10^{14}$ Pa s. (c) As for Figure 4b but for $\eta_0 = 10^{13}$ Pa s.

brittle zone exceeds the rheologically determined temperature T_D. Thus, although the analytical model used by *Stevenson* [1996] is appropriate to Europa if $D \geq \sim 4$ km, we consider it unlikely that moving shear zones will develop long-term brittle thicknesses that are this large. In our models, values of D are unlikely to exceed 2 km if shear motion persists for longer than $\sim 10^5 a$, and melt generation is likely at shear velocities greater than or equal to $\sim 10^{-6}$ m s^{-1}. Such shear velocities are likely only if Europa is deforming at diurnal timescales and imply a geologically active satellite; at present, no ongoing geological activity has been detected [*Phillips et al.*, 2000].

[40] It is important to examine the robustness of these conclusions to the considerable uncertainties in the parameters. Although neither the width nor the depth of the real situation on Europa is well constrained, the model box depth h does not have a significant effect if brittle heating is dominant. We found that for the case in Table 1, increasing h from 20 km to 30 km increased the temperature anomaly by 2 K at $u_0 = 10^{-8}$ m s^{-1} and 14 K at $u_0 = 10^{-6}$ m s^{-1}. For the base case, increasing the box width by a factor of 2 changes the maximum temperature by <5%. Changing the width of the surface deforming zone, x_l, by a factor of 3 changes the maximum temperature by <0.5% in the base case. Hence the results presented above are relatively insensitive to the exact dimensions used in the model. On the other hand, they are highly sensitive to the assumed velocity and rheology. For instance, increasing Q to 30 kJ mol^{-1} increases the temperature anomaly from 66 K to 78 K, roughly in line with equation (10). The effect of changing η_0 is also considerable, as seen in Figures 4 and 5.

[41] *Head et al.* [1999] speculated that shear zone heating might lead to diapirism and uplift. Our results show that the heating, and hence the lateral temperature contrasts, are greatest at the base of the brittle layer. Assuming that a rising diapir can be modeled as a Stokes body, using a near-surface viscosity value of $\sim 10^{17}$ Pa s and a density contrast of 10 kg m^{-3} results in a vertical velocity of a few centimeters per year. This velocity will produce substantial displacement if the strike-slip zones are active over even a small fraction of the estimated surface age of ~ 50 Myr [*Pappalardo et al.*, 1999]. Thus zones of viscous dissipation are natural places to expect to see evidence of diapiric activity. The expected vertical

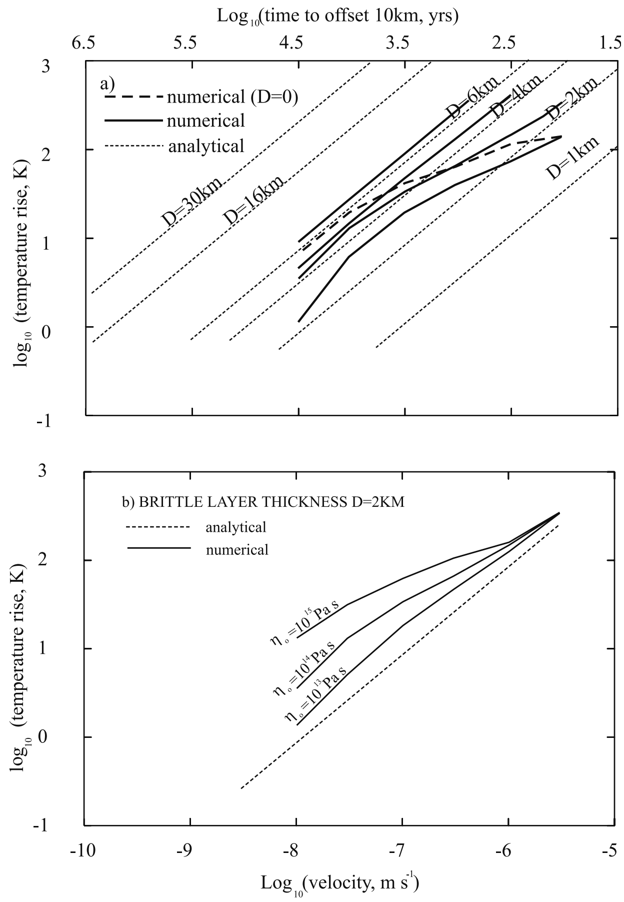

Figure 5. (a) Maximum temperature anomaly as a function of shear velocity and brittle layer thickness, D. Solid lines are from numerical model, bold dashed line is from numerical model with $D = 0$, and thin dashed lines are from analytical solution (equation (4)). Parameters used in model are given in Table 1. Velocity plotted is $u_0/2$. (b) Effect of ductile zone reference viscosity on temperature anomaly. Solid lines are numerical results using different values of η_0 and $D = 2$ km; dashed line is analytical result for purely brittle case using equation (4).

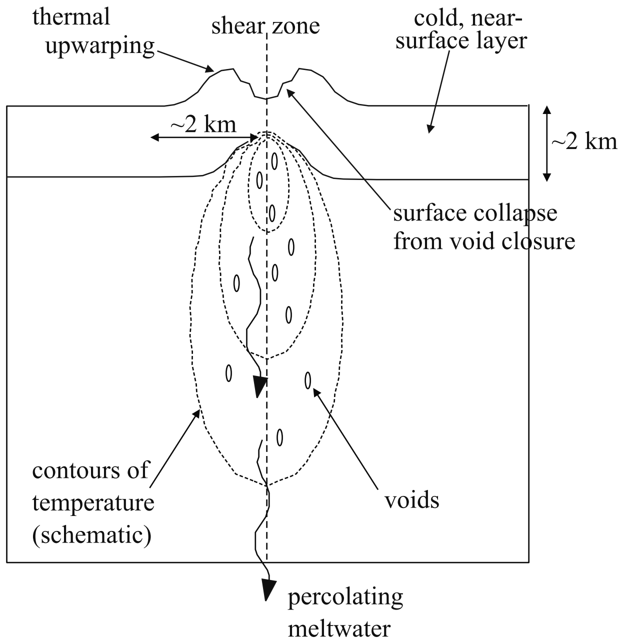

Figure 6. Schematic diagram of effects of shear motion within ice crust. Dashed lines are schematic contours of excess temperature. The removal of water by percolation results in voids. Closure of the voids causes surface collapse; the temperature anomaly causes flexural uplift. Alternatively, inward motion of the ice due to void closure may lead to compression and uplift (see text).

velocity value is slower than the strike-slip velocities that cause such temperature anomalies and thus justifies the neglect of vertical velocities in the original formulation. We note, however, that if convection is occurring [*Pappalardo et al.*, 1998; *McKinnon*, 1999], our assumptions of conductive heat transfer and zero vertical velocity will not be correct.

[42] Even if the near-surface ice viscosity is too high to allow appreciable diapiric motion, the warm ice will still be buoyant and thus exert an upward stress. The resulting flexural uplift s will be approximately given by [*Turcotte and Schubert*, 1982]

$$s \sim r^2 \alpha \, \Delta T \left(\frac{\rho g}{D}\right)^{1/4}, \tag{16}$$

where r is the characteristic length scale of the buoyant ice, α is the thermal expansivity ($= 1.4 \times 10^{-4}$ K^{-1}), ΔT is the temperature contrast, and D is the flexural rigidity. Assuming an elastic thickness of 0.5 km [*Williams and Greeley*, 1998], a Young's modulus of 1 GPa [*Vaughan*, 1995], $r = 5$ km, and $\Delta T = 50$ K results in a flexural uplift of $\sim$100 m. The lateral extent of the uplift is controlled by the flexural parameter and in this case will be $\sim$2 km. Both the vertical and lateral extent of the predicted uplift are similar to the observed double ridge characteristics [*Giese et al.*, 1999].

[43] In both cases, cessation of strike-slip motion will cause the uplift to decay over the thermal diffusion timescale ($\sim 10^5 a$). Thus, if either explanation is correct, ridges are indicative of recent strike-slip motion. However, as pointed out below, if melting occurs, the ridges may not be supported by thermal effects and thus do not have to be recent features.

[44] We demonstrated above that velocities in excess of $\sim 10^{-6}$ m s^{-1} may result in melting, at rates of $\sim 10^{-6}$–10^{-5} m^2 s^{-1}. *Gaidos and Nimmo* [2000] argued that melt fractions greater than $\sim$1% will allow the water to percolate downward as rapidly as it is produced. If melt is being generated and continuously removed to the interior, voids will be formed. The draining of melt downward may lead to vertical motion of the matrix, resulting in local thinning of the crust and sagging at the surface. The voids may also be partly closed by inward motion of the ice, in which case compression will result. The downward sagging, accompanied by either thermal or compression-induced upwarping, may be responsible for the formation of double ridges on Europa (see Figure 6). Ridges formed by the compression mechanism are not thermally supported and will thus persist once strike-slip motion has ceased.

[45] There are a number of ways in which our analysis of melting is unlikely to be correct in detail. First, the assumption of a constant brittle layer thickness D is unlikely to be correct, as discussed above. However, even in the complete absence of a brittle layer, melt will still be generated for sufficiently large velocities, as shown by Figure 5a. *Gaidos and Nimmo* [2000] estimated that velocities of order 10^{-6} m s^{-1} were sufficient to generate melt in the purely ductile case, and application of equation (10) results in a center temperature of 270 K (i.e., melting) for a velocity of 7×10^{-6} m s^{-1} if the center viscosity is 10^{13} Pa s.

[46] Second, the generation and motion of melt advects heat, which is not dealt with in equation (8). For instance, the water that is percolating downward may freeze once it reaches cold ice (see Figure 3), releasing latent heat and thus altering the temperature distribution. Third, ice undergoes a reduction in viscosity near the solidus [*De La Chapelle et al.*, 1999]; however, incorporating this effect into equation (7) altered the temperature anomaly by <10 K for the base case, and the effect was therefore neglected. In reality, for pure ice the temperature should never exceed the solidus while melting is occurring. For the brittle ice layer the coefficient of friction is likely to be decreased once melting starts, leading to possible periodic heating and motion. Thus the melt generation rates are subject to considerable uncertainty, although the qualitative behavior as the solidus is approached is likely to be correct.

[47] The calculations above (Figure 3) show that the shear stresses required to maintain a viscous shear zone are comparable to likely present-day Europa tidal stresses. We have not shown here that such a zone can be initiated; in particular, static friction along a preexisting fault may require shear stresses exceeding the likely tidal stresses. Furthermore, future models should solve for the time-dependent evolution of the shear zone and the thickness of the overlying brittle crust in a time-dependent fashion. Finally, the explanation for the formation of double ridges proposed here requires diurnal motion. Although such motion is possible given the present-day tidal stresses, alternative explanations [*Head et al.*, 1999; *Greenberg et al.*, 1998] may not require such high strain rates.

7. Conclusions

[48] Strike-slip motion is common on Europa and is likely to produce localized shear heating. For reasonable rheological parameters the present-day tidal shear stresses on Europa are probably sufficient to cause motion and heating. If the fault motion occurs on diurnal timescales, it is likely to cause melt generation. The heating may lead to thermal uplift around the shear zone; the melting will cause subsidence and possibly compression at the shear zone. These two mechanisms together may explain the preponderance of double ridges on the surface.

Appendix A: Verifying the Model

[49] We verified that our model could reproduce the analytical results for both purely brittle (equation (4)) and purely ductile (equation (10)) situations. For the purely brittle case we assumed a constant initial temperature throughout the region and a value of D

of one third the box depth and constrained the velocity to be zero everywhere below the fault. With 31 nodes in the x and z directions we found that the numerical solution agreed with the analytical solution to within 0.5% for $\Delta x = \Delta z = 1.0$ km. The numerical solution became less accurate as Δx increased with Δz held constant but still agreed within 10% for $\Delta x = 4$ km.

[50] For the purely viscous case we set $D = 0$, $\partial T/\partial z = 0$, and $\partial u/\partial z = 0$ at the top and bottom boundaries and specified the side boundaries and initial internal temperature to be T_0. These conditions effectively reduce the problem to one dimension. We then proceeded to solve the numerical problem for various grid resolutions and compared the calculated maximum temperature increase with that given by equation (10). The model reproduced the analytical result to within 1% except for the lowest resolution grid used (5 nodes). Varying the grid spacing, either independently or together, by a factor of 3 resulted in <0.1% change in the numerical result.

[51] The grid parameters used for various models are given in Table 2. For our base case ($D = 2$ km, $h = 20$ km), doubling the number of nodes used in each dimension produced less than a 2% change in the maximum temperature. Increasing Δx by a factor of 2 had a 4% effect on the maximum temperature. We found that convergence was generally reached within 10^5 time steps, except in cases where melt was generated (see below). The reason that this model reaches steady state, whereas the temperature profiles in *Yuen et al.* [1978] increase with the square root of time, is that our model has a fixed temperature at the side boundaries.

[52] **Acknowledgments.** F.N. thanks the California Institute of Technology, Magdalene College, Cambridge, and the Royal Society for their financial support. We also thank Moses Milazzo for his review.

References

Abramowitz, M., and I. A. Stegun, *Handbook of Mathematical Functions*, Dover, Mineola, N. Y., 1970.

Brace, W. F., and D. L. Kohlstedt, Limits on lithospheric stress imposed by laboratory experiments, *J. Geophys. Res.*, *85*, 6248–6252, 1980.

Carr, M. H., et al., Evidence for a subsurface ocean on Europa, *Nature*, *391*, 363–365, 1998.

Chen, W.-P., and P. Molnar, Focal depths of intracontinental and intraplate earthquakes and their implications for the thermal and mechanical properties of the lithosphere, *J. Geophys. Res.*, *88*, 4183–4214, 1983.

De La Chapelle, S., H. Milsch, O. Castelnau, and P. Duval, Compressive creep of ice containing a liquid intergranular phase: Rate controlling processes in the dislocation creep regime, *Geophys. Res. Lett.*, *26*, 251–254, 1999.

Durham, W. B., S. H. Kirby, and L. A. Stern, Creep of water ices at planetary conditons: A compilation, *J. Geophys. Res.*, *102*, 16,293–16,302, 1997.

Fleitout, L., and C. Froidevaux, Thermal and mechanical evolution of shear zones, *J. Struct. Geol.*, *2*, 159–164, 1980.

Gaidos, E., and F. Nimmo, Tectonics and water on Europa, *Nature*, *405*, 637, 2000.

Giese, B., R. Wagner, G. Neukum, R. Sullivan, and the SSI Team, Doublet Ridge Formation on Europa: Evidence from topographic data, paper presented at 31st Annual Meeting of the Division for Planetary Sciences, Am. Astron. Soc., Padova, Italy, 1999.

Goldsby, D. L., and D. L. Kohlstedt, Superplastic deformation of ice: Experimental observations, *J. Geophys. Res.*, *106*, 11,017–11,030, 2001.

Golombek, M. P., and W. B. Banerdt, Constraints on the subsurface structure of Europa, *Icarus*, *83*, 441–452, 1990.

Greenberg, R., et al., Tectonic processes on Europa: Tidal stresses, mechanical response and visible features, *Icarus*, *135*, 64–78, 1998.

Head, J. W., R. T. Pappalardo, and R. Sullivan, Europa: Morphological characteristics of ridges and triple bands from Galileo data (E4 and E6) and assessment of a linear diapirism model, *J. Geophys. Res.*, *104*, 24,223–24,236, 1999.

Hoppa, G., B. R. Tufts, R. Greenberg, and P. Geissler, Strike-slip faults on Europa: Global shear patterns driven by tidal stress, *Icarus*, *141*, 287–298, 1999.

Hoppa, G., R. Greenberg, B. R. Tufts, P. Geissler, C. Phillips, and M. Milazzo, Distribution of strike-slip faults on Europa, *J. Geophys. Res.*, *105*, 22,617–22,627, 2000.

Jacobson, H. P., and C. F. Raymond, Thermal effects on the location of ice stream margins, *J. Geophys. Res.*, *103*, 12,111–12,122, 1998.

Kennedy, F. E., E. M. Schulson, and D. E. Jones, *Philos. Mag. A*, *80*, 1093–1110, 2000.

Kivelson, M. G., et al., Galileo magnetometer measurements: A stronger case for a subsurface ocean at Europa, *Science*, *289*, 1340–1343, 2000.

Lockett, J. M., and N. J. Kusznir, Ductile shear zones: Some aspects of constant slip velocity and constant shear stress models, *Geophys. J. R. Astron. Soc.*, *69*, 477–494, 1982.

McKinnon, W. B., Convective instability in Europa's floating ice shell, *Geophys. Res. Lett.*, *26*, 951–954, 1999.

McKinnon, W. B., Europan heat flow and crustal thickness estimates from fold wavelengths and impact ring graben widths, paper presented at 32nd Annual Meeting of the Division for Planetary Sciences, Am. Astron. Soc., Pasadena, Calif., 2000.

Ojakangas, G. W., and D. J. Stevenson, Thermal state of an ice shell on Europa, *Icarus*, *81*, 220–241, 1989.

Pappalardo, R. T., et al., Geological evidence for solid-state convection in Europa's ice shell, *Nature*, *391*, 365–367, 1998.

Pappalardo, R. T., et al., Does Europa have a subsurface ocean? Evaluation of the geological evidence, *J. Geophys. Res.*, *104*, 24,015–24,055, 1999.

Phillips, C. B., et al., The search for current geologic activity on Europa, *J. Geophys. Res.*, *105*, 22,579–22,597, 2000.

Press, W. H., S. A. Teukolsky, W. T. Vetterling, and B. P. Flannery, *Numerical Recipes*, Cambridge Univ. Press, New York, 1992.

Schubert, G., T. Spohn, and R. T. Reynolds, Thermal histories, compositions and internal structures of the moons of the solar system, in *Satellites*, edited by J. A. Burns and M. S. Matthews, pp. 224–292, Univ. of Ariz. Press, Tucson, 1986.

Sibson, R. H., Fault zone models, heat flow, and the depth distribution of earthquakes in the continental crust of the United States, *Bull. Seismol. Soc. Am.*, *72*, 151–163, 1982.

Stevenson, D. J., Heterogeneous tidal deformation and geysers on Europa, in *Europa Ocean Conference, Capistrano Conf. 5*, pp. 69–70, San Juan Capistrano Res. Inst., San Juan Capistrano, Calif., 1996.

Tufts, B. R., R. Greenberg, G. Hoppa, and P. Geissler, Astypalaea Linea: A large-scale strike-slip fault on Europa, *Icarus*, *141*, 53–64, 1999.

Turcotte, D. L., and E. R. Oxburgh, A fluid theory for the deep structure of dip-slip fault zones, *Phys. Earth Planet. Inter.*, *1*, 381–386, 1968.

Turcotte, D. L., and G. Schubert, *Geodynamics*, J. Wiley, New York, 1982.

Vaughan, D. G., Tidal flexure at ice shell margins, *J. Geophys. Res.*, *100*, 6213–6224, 1995.

Williams, K. K., and R. Greeley, Estimates of ice thickness in the Conamara Chaos region of Europa, *Geophys. Res. Lett.*, *25*, 4273–4276, 1998.

Yuen, D. A., L. Fleitout, G. Schubert, and C. Froidevaux, Shear deformation zones along major transform faults and subducting slabs, *Geophys. J. R. Astron. Soc.*, *54*, 93–119, 1978.

E. Gaidos, Department of Geology and Geophysics, University of Hawaii, Honolulu, HI 96822, USA. (gaidos@soest.hawaii.edu)

F. Nimmo, Department of Geological Sciences, University College London, Gower Street, London WC1E 6BT, UK. (nimmo@gps.caltech.edu)